

1 **An Intertropical Convergence Zone shift controlled the terrestrial material supply on the Ninetyeast Ridge**

2 *Xudong Xu^{1,3,4}, Jianguo Liu^{1,2,4,*}, Yun Huang^{1,*}, Lanlan Zhang^{1,4}, Liang Yi⁵, Shengfa Liu^{2,6}, Yiping Yang^{1,4}, Li Cao⁷, Long*
3 *Tan^{1,3,4}*

4 ¹Key Laboratory of Ocean and Marginal Sea Geology, South China Sea Institute of Oceanology, Chinese Academy of
5 Sciences, Guangzhou 510301, China

6 ²Laboratory for Marine Geology, Pilot National Laboratory for Marine Science and Technology, Qingdao 266061, China

7 ³University of Chinese Academy of Science, Beijing 100049, China

8 ⁴Southern Marine Science and Engineering Guangdong Laboratory (Guangzhou), Guangzhou 511458, China

9 ⁵State Key Laboratory of Marine Geology, Tongji University, Shanghai 200092, China

10 ⁶Key Laboratory of Marine Geology and Metallogeny, First Institute of Oceanography, Ministry of Natural Resources,
11 Qingdao 266061, China

12 ⁷Shandong Provincial Research Institute of Coal Geology Planning and Exploration, Jinan 250104, China

13 Corresponding authors: Jianguo Liu (jgliu@scsio.ac.cn) and Yun Huang (huangyun@scsio.ac.cn)

14 **Abstract**

15 Among various climate drivers, direct evidence for the Intertropical Convergence Zone (ITCZ) control of sediment supply
16 on the millennial scale is lacking, and the changes in ITCZ migration demonstrated in paleoclimate records need to be
17 better investigated. Here, we use clay minerals and Sr-Nd isotopes obtained from a gravity core on the Ninetyeast Ridge
18 to track the corresponding source variations and analyze the relationship between terrestrial material supply and climatic
19 changes. On the glacial-interglacial scale, chemical weathering weakened during the North Atlantic cold climate periods
20 and falling sea level hindered the transport of smectite into the study area due to the exposure of Andaman and Nicobar
21 Islands. However, the influence of the South Asian monsoon on the sediment supply was not obvious on the millennial
22 scale. We suggest that the north-south migration of the ITCZ controlled the rainfall in Myanmar and further directly

23 determined the supply of clay minerals on the millennium scale because the transport of smectite was highly connected
24 with the ITCZ location; thus, the regional shift of the ITCZ induced an abnormal increase in the smectite percentage during
25 the late Last Glacial Maximum (LGM) in our records. The smectite percentage in the studied core is similar to distinct
26 ITCZ records but different in some periods, revealing that regional changes in the ITCZ were significantly obvious and
27 that the ITCZ is not a simple north-south displacement and closer connections occurred between the Northern-Southern
28 Hemispheres in the eastern Indian Ocean during the late LGM.

29 **1. Introduction**

30 Deposited sediments are essential recorders of the paleoclimate and paleoceanographic conditions since the climate is tied
31 to the whole sedimentation process from weathering and transport to the deposition of sediments on land. The terrestrial
32 materials of "source-sink" systems are supplied to marine environments under the combined effects of multiple climate-
33 related driving forces and ocean processes (Li et al., 2018; Yu et al., 2019), and understanding these effects is crucial for
34 reconstructing the coevolutionary relationship of the palaeoenvironment with the palaeoceanographic conditions and
35 palaeoclimate. Various factors may control the formation and transport of terrestrial materials at low latitudes, such as the
36 northeastern Indian Ocean. Recently, the South Asian monsoon has been revealed to be the main driving force of terrestrial
37 material supply in Bangladesh and of hydrological changes in the Bay of Bengal (BoB, Dutt et al. al., 2015; Gebregiorgis
38 et al., 2016; Jousain et al., 2017; Li et al., 2018; Liu et al., 2021). Moreover, the Intertropical Convergence Zone (ITCZ)
39 is an important climate-driving force in low-latitude regions (Deplazes et al., 2013; Ayliffe et al., 2013), which has a pivotal
40 role in heat transportation on Earth (Schneider et al., 2014), and the north-south shift of the ITCZ is thought to connect the
41 climates in the Northern and Southern Hemispheres (Huang et al., 2019; Zhuravleva et al., 2021). Because monsoon
42 dynamics are shaped by large-scale meridional temperature gradients and an ITCZ shift in tropical monsoon areas (Mohtadi
43 et al., 2016), there are hopeful opportunities to analyze sediment responses to ITCZ or monsoon variations. The
44 paleoclimate breakthroughs mentioned above enable us to analyze the response of sedimentary records to the ITCZ shift

45 in the BoB more accurately. However, evidence for direct control of terrestrial sediment supply by the ITCZ remains
46 lacking, which is an obstacle to understanding the response of the depositional environment to the ITCZ shift.

47 As the main deposition area for vast amounts of weathered Himalayan materials, the BoB accumulates numerous
48 Himalayan terrestrial materials that are loaded by the Ganges-Brahmaputra (G-B) River (Goodbred and Kuehl, 2000) and
49 forms the largest subaqueous fan, the Bengal Fan (3000 km long from north to south, 1400 km wide from east to west,
50 with an area of 3.9×10^5 km²; Curray et al., 2003). The eastern and western sides of the BoB correspond to the Andaman
51 Sea and the Indian Peninsula, respectively, and the BoB is a natural site that is useful for studying the interactions between
52 weathering and climatic factors since both sides of the bay are affected by the South Asian monsoon (Ali et al., 2015).
53 Previous studies suggest that Himalayan material transported by the G-B River was the predominant source of material in
54 the northern BoB (Li et al., 2018; Ye et al., 2020), and the main sources in the west BoB are the Indian Peninsula and
55 Himalayan weathered material (Kessarkar et al., 2005; Tripathy et al., 2011; Tripathy et al., 2014). In the eastern BoB, the
56 sediment source areas include the Himalayan (transported by the G-B river), Indo-Burman Ranges and the Myanmar region
57 through which the Irrawaddy River flows (Colin et al., 1999; Jousain et al., 2016). The terrigenous detrital material in the
58 Andaman Sea is mainly Myanmar-origin sediments transported by the Irrawaddy River (Ali et al., 2015; Awasthi et al.,
59 2014; Colin et al., 2006). A series of terrigenous sediment issues, such as changes in the source area and proportion of
60 terrigenous matter in various regions of the BoB from the LGM to the Holocene, the distribution range of terrigenous
61 materials in the western and eastern BoB, and how the G-B River sediments are transported in the BoB, are unclear until
62 now. Little attention has been given to sediment provenance in the southern BoB or, particularly, to the correlation of these
63 sediment sources with climatic driving factors.

64 Recent studies have revealed that clay minerals can be used to effectively track changes in source areas in the source-
65 sink system of the BoB due to the great differences in clay mineral components among the source areas around the BoB
66 (Jousain et al., 2016; Li et al., 2017; Liu et al., 2019; Ye et al., 2020). Moreover, Sr-Nd isotopes have been widely reported

67 to track the variations in sediment provenance in the BoB (Ahmad et al., 2005; Colin et al., 1999; Colin et al., 2006).

68 In this study, we measured clay minerals and Sr-Nd isotopes in a deep-sea gravity core obtained from the southeastern
69 BoB (Figure 1) to reconstruct variations in the sources of sediments in the Ninetyeast Ridge and to further explore the
70 climate forces that affected the supply of terrestrial materials during the past 45 ka. Core 17I106 located above the abyssal
71 plain at ~900 m, exempting from the influence of large-scale turbidite activities and receiving only fine-grained pelagic
72 sediments that can reflect the changes in the provenance of the surrounding source area (Figure 1), which makes the
73 terrestrial sediments on the Ninetyeast Ridge suitable for exploring the relationship between the paleoclimate and
74 paleoenvironment in the BoB. Here, we aim to disentangle the ITCZ variability signal in marine sediments from multiple
75 driving forces and further understand the response of sedimentary records to ITCZ migrations.

76 **2. Materials and methods**

77 **2.1. Chronology**

78 Gravity core 17I106 (90.0040°E, 6.2105°N, water depth 2928 m) was collected by the *R/V Shiyan 1* vessel belonging to
79 the South China Sea Institute of Oceanology (SCSIO), Chinese Academy of Sciences (CAS), from the Ninetyeast Ridge,
80 northeast of the Indian Ocean (Figure 1). This core has a total length of 162 cm and consists of gray to green silty clays
81 subsampled at 1-cm intervals. The age model of core 17I106 was reconstructed based on 10 accelerator mass spectrometry
82 (AMS) ¹⁴C dates and Bayesian interpolations between these dates (Figure 2 and Table 1). AMS ¹⁴C dating was performed
83 on mixed planktonic foraminifera at Beta Analytic Inc. More than 20 mg of intact mixed planktonic foraminifera shells
84 were selected from the >150 μm fractions of each sample (10 g dried sample). All radiocarbon ages were converted and
85 reported as calendar years before present with the Calib8.2 software program with the Marine20 calibration dataset (Reimer
86 et al., 2020). A continuous depth-age model was performed using Bacon software by dividing a sedimentary sequence into
87 many thin segments and estimating a linear accumulation rate for each segment based on the calibrated ¹⁴C dates and a

88 Bayesian approach (Blaauw and Christen, 2011).

89 **2.2. Clay mineralogy**

90 Clay minerals (<2 μm) were separated from the sediment samples by sedimentation according to Stokes' settling velocity
91 principle after organic materials and carbonates were removed with 15% hydrogen peroxide (H_2O_2) and 0.1 N hydrochloric
92 acid (HCl), respectively. We used the sedimentation method by placing the sample in glassware with an inner diameter of
93 7 cm and a height of 10 cm at an experimental temperature of 19 °C. The sedimentation time was calculated as 4 hours and
94 10 minutes according to Stokes' formula. The upper 5 cm of liquid was extracted, followed by centrifugation at 4800 rpm
95 for 10 minutes, and the smear was made into a natural slice. The natural slice was heated in an oven at 60 °C for 24 hours
96 to make ethylene glycol saturated slides for the subsequent test. The clay mineral slides were measured using routine X-
97 ray diffraction (XRD) equipment (Bruker Inc, D8 ADVANCE) in the Key Laboratory of Ocean and Marginal Sea Geology,
98 SCSIO, CAS. Clay mineral abundance was calculated by measuring the peak areas of smectite (15-17 Å), illite (10 Å) and
99 kaolinite/chlorite (7 Å). Relative proportions of kaolinite and chlorite were calculated from the ratio of 3.57 Å/3.54 Å peak
100 areas. The relative percentages of the four main clay minerals were estimated by calculating the integrated peak areas of
101 characteristic basal reflections using Topas5P software with the empirical factors by Biscaye (1965). The reproducibility
102 error of this method is \pm 5-10%.

103 **2.3 Sr-Nd isotope analyses**

104 Twenty-two samples (<63 μm) from core 17I106 were selected for isotope analyses, and we used the experimental method
105 described by Dou et al. (2016). Carbonates were removed from 70 to 100 mg powdered bulk samples by leaching with
106 0.25 N HCl for 24 h at 50 °C. The residues were then completely digested in high-pressure Teflon bombs using a HCl +
107 $\text{HNO}_3 + \text{HClO}_4 + \text{HF}$ solution. Rb and Sr were separated in 2.5 N HCl using Bio-Rad AG50W-X12, 200–400 mesh cation
108 exchange resin. Sm and Nd were separated in 0.15 N HCl using P507 cation exchange resin. The strontium (Sr) and

109 neodymium (Nd) isotopic compositions of the sediment samples were measured using a Thermo Scientific Multi-Collector
110 Inductively Coupled Plasma Mass Spectrometer (MC-ICPMS Nu plasma) at the Key Lab of Marine Sedimentology and
111 Environmental Geology, Ministry of Natural Resources, China. The organic materials and carbonate were removed from
112 the samples by H₂O₂ and HCl, respectively. For the convenience of direct comparison, the Nd isotopic ratio results are
113 expressed as $\epsilon\text{Nd}(0) = [({}^{143}\text{Nd}/{}^{144}\text{Nd})_{\text{meas}}/0.512638 - 1] * 10000$, using the present CHUR value (Jacobsen and Wasserburg,
114 1980). Replicate analyses of NBS-987 during the study gave a mean ${}^{87}\text{Sr}/{}^{86}\text{Sr}$ of 0.710310 ± 0.000003 (2s), close to its
115 certified value of 0.710245. Similarly, replicate analyses of JNDi-1 gave a mean ${}^{143}\text{Nd}/{}^{144}\text{Nd}$ of 0.512112 ± 0.000004 (2s),
116 and its certified value was 0.511860.

117 3. Results

118 The age model is built based on 10 radiocarbon dates from core 17I106. The top age is 3.8 ka BP, and the bottom age is
119 44.9 ka BP; thus, this core covers a continuous sedimentary succession of the last ~45,000 years. The sedimentation rates
120 in the Holocene (average 3.1 cm/ka) were relatively lower than those during the last glacial period (average 4.6 cm/ka),
121 with the highest rate of 8.3 cm/ka during 12.5–13.6 ka BP (Figure 3a). In the study core, the illite percentage ranges from
122 31% to 63% with an average of 48%, while the smectite percentage ranges between 8% and 57% with an average of 30%
123 (Figure 3b-e). Moreover, the kaolinite percentage ranges from 2% to 16%, and the chlorite percentage ranges from 5% to
124 20% in the core sediments. In the study core, the ${}^{87}\text{Sr}/{}^{86}\text{Sr}$ ratios range from 0.7122015 to 0.7186141 with an average of
125 0.7161698, while ϵNd values range from -13.02 to -10.29 with an average of -11.24 (Figure 3f-g). At this study core, the
126 ${}^{87}\text{Sr}/{}^{86}\text{Sr}$ ratio and ϵNd values remain stable before the LGM but show fluctuations after the LGM, without obvious
127 increasing/decreasing tendencies. During ~14.5-12.5 ka, ${}^{87}\text{Sr}/{}^{86}\text{Sr}$ ratios significantly increased from 0.7139 to 0.7172,
128 while ϵNd values decreased abruptly from -10.28 to -13.02.

129 4. Discussion

130 **4.1. Sediment provenance and transport patterns**

131 The lower sedimentation rates (3-5 cm/ka, Figure 3a) measured in core 17I106 were in accordance with the normal
132 sedimentation rates obtained from neighboring cores around the Ninetyeast Ridge (Ahmad et al., 2005; Raza et al., 2013).
133 In this region, turbidite activities were less developed (Joussain et al., 2016; Fournier et al., 2017), in accordance with its
134 far distance from the Active Channel (Figure 1). In the northern BoB, due to heavy river runoff and steep topography, the
135 G-B river system transports a large amount of the products of Himalayan physical denudation; these products mainly
136 consist of illite and chlorite formed under dry and cold climate conditions (Chamley, 1989; Khan et al., 2019). Because of
137 the hot and humid conditions in Myanmar and the Indian Peninsula, sediments in these regions are formed through the
138 chemical weathering of silicate minerals and thus have high smectite percentages. Moreover, the Irrawaddy River brought
139 weathered products characterized by high smectite percentages from Myanmar into the Andaman Sea, leading to high
140 smectite percentages in the terrestrial sediments deposited in this marine environment (Ali et al., 2015).

141 The relatively high illite percentages measured in core 17I106 indicate that the weathered Himalayan materials carried
142 by the G-B River system are the primary source of sediments in the study area (Figure 4a). Compared with the large
143 amounts of materials loaded by the G-B River system, the weathered areas and runoff volumes of the Indo-Burman Ranges
144 are relatively small, and consequently, their sediment contributions are limited in the study area, although their sediments
145 are also characterized by relatively high illite percentages (Joussain et al., 2016). Evidence of surface sediments in the BoB
146 further reveals that the smectite percentages of sediments in the central region are significantly lower than those in the
147 eastern and western regions (Li et al., 2017; Liu et al., 2019), indicating that sediments of Indian Peninsula origin are
148 difficult to transport into the eastern BoB through the central BoB. Because the limited weathering area of Andaman and
149 Nicobar Islands cannot provide a large amount of smectite according to provenance studies (Ali et al., 2015), the Myanmar
150 materials characterized by high smectite percentages have the advantage of shorter transport distances compared to those
151 sourced from the Indian Peninsula as the main source area of smectite around the BoB. Therefore, the most important

152 source of smectite in the study area is the Myanmar region. In marine environments, kaolinite is preferentially deposited
153 in estuary areas due to mineral segregation (Gibbs, 1977) and thus may not be transported over long distances, so the
154 kaolinite in the study area was most likely sourced from neighboring Sumatra (Figure 4a, Liu et al., 2012). The Sr-Nd
155 isotopes measured in the studied core are close to those measured in the Irrawaddy/Indo-Burman Ranges/Sumatra source
156 regions (Figure 4b), indicating that terrestrial materials with diameters $<63 \mu\text{m}$ mainly come from the Irrawaddy River,
157 Indo-Burman Ranges and Sumatra source areas, which was confirmed by a Sr-Nd isotope study in the southwestern part
158 of the study area (Ahmad et al., 2005) and consistent with sediment provenance studies in the Ninetyeast Ridge on different
159 timescales (Ali et al., 2021; Seo et al., 2022). This difference in clay minerals and isotopes may be consistent with the view
160 that clay minerals may be transported over long distances, while coarser terrestrial sediments can only be transported to
161 more proximate locations.

162 In the northeastern BoB, the southwest monsoon turns southward into the Andaman Sea, resulting in the transport of
163 sediments from the Indo-Burman Range and Irrawaddy River to the central Andaman Sea (Colin et al., 2006). The location
164 of core 17I106, drilled on the Ninetyeast Ridge, was above the abyssal plain, and the terrestrial materials deposited to the
165 west of this location are difficult to resuspend and deposit on the ridge under the force of bottom currents or turbidity
166 currents. In fact, the G-B River-loaded materials are mainly carried eastward by surface ocean currents in summer to the
167 Andaman Sea, where the seasonal surface currents load materials from the Himalayan and Indo-Burman Ranges into the
168 Andaman Sea through the northern strait (NS) (Liu et al., 2020a; Rayaroth et al., 2016). These G-B River sediments can
169 also be transported southward along the west side of the Andaman and Nicobar Islands (Figure 5), and a westward ocean
170 surface current in the middle strait (MS) loads sediments of the Irrawaddy River southwest into the study area (Chatterjee
171 et al., 2017).

172 **4.2. Factors affecting sediment provision**

173 In general, illite is the major mineral produced during the strong physical erosion of metamorphic rocks and granite rocks

174 and during the reprocessing of sedimentary rocks (Chamley, 1989; Winkler et al., 2002), while smectite is the secondary
175 mineral produced during the chemical weathering of parent aluminosilicate and iron-magnesium silicate under warm and
176 humid climate conditions (Chamley, 1989; Erosion, 1995). The climatic forces from the North Atlantic are thought to
177 extensively impact the tropical Eastern Indian Ocean (EIO) and surrounding areas of the BoB (Sun et al., 2011; DiNezio
178 and Tierney, 2013; Dutt et al., 2015; Gautam et al., 2020; Mohtadi et al., 2014; Liu et al., 2021), whose climate signals can
179 be transmitted via the tropical Atlantic bipolar SST anomaly and associated southward shift of the ITCZ (Marzin et al.,
180 2013), westerlies teleconnection and sea ice (Sun et al., 2011) or the reorganization of the Hadley circulation (Mohtadi et
181 al., 2014). During the North Atlantic cold-climate periods (Heinrich events and YD period, Figure 3h), when rainfall and
182 temperatures decreased in the South Asian monsoon region (An et al., 2011; DiNezio and Tierney, 2013; Gautam et al.,
183 2020), physical weathering was enhanced in the Himalayas (Joussain et al., 2016), which made illite percentages at core
184 17I106 relatively high during these cold-climate periods, but chemical weathering weakened in Myanmar, and the smectite
185 percentage thus decreased in the source area before these cold periods and continued to increase after these periods. The
186 increasing (decreasing) trend of illite (smectite) percentages before cold-climate periods and the decreasing (increasing)
187 trend of illite (smectite) percentages after cold-climate periods in our records suggest that the weathering degree in the
188 source area influenced the supply of clay minerals during these cold-climate periods.

189 Sea level fluctuation is also critical in controlling the supplementation of terrestrial materials, especially clay minerals
190 (Li et al., 2018; Liu et al., 2019), by changing the transport paths and/or distances as well as the further input of sediments
191 into the study area. The changing trends of the sea level in seas adjacent to the BoB (Figure 3i, Waelbroeck et al., 2002;
192 Grant et al., 2014; Hanebuth et al., 2000; Thompson and Goldstein, 2006) are well correlated with the smectite percentages
193 measured in core 17I106, especially during 35-21 ka, when the smectite percentages declined continuously. Since the
194 Andaman and Nicobar Islands connecting the Andaman Sea and the BoB have continuously expanded as the sea level has
195 continuously declined, the strait width has been consistently reduced, thereby preventing the entrance of terrestrial

196 materials into the Andaman Sea and the further continuous decline in smectite percentages in the study area. Here, we
197 suggest that the variations in the measured illite percentages were mainly caused by changes in smectite deposition because
198 the sedimentary records obtained from the northern BoB do not support the controlling effect of sea level on illite
199 percentages over the past 50 ka (Joussain et al., 2016; Li et al., 2018; Liu et al. al., 2019). The relative exposure of 200 km
200 from the current Irrawaddy River delta may affect the deposition process on the continental shelf or further deposition of
201 the sediments delivered to the deep ocean, but core 17I106 is formed by the long-distance transport of large amounts of
202 fine-grained terrestrial material, indicating that these sediments can be transported over long distances, and the ~200 km
203 change in the shelf distance is not a dominant factor of sediment transport in the study area. Moreover, the decreasing
204 smectite percentages from the Myanmar area as sea level decreases suggests that shelf denudation is also not the main
205 factor affecting our smectite record, which is in accordance with previous studies in the Andaman Sea that have not
206 specifically emphasized the alteration of terrestrial source material supply by exposed shelves (Ali et al., 2015; Awasthi et
207 al., 2014).

208 The South Asian summer monsoon is normally thought to be an important factor affecting weathering conditions
209 around the BoB (Dutt et al., 2015; Gebregiorgis et al., 2016; Joussain et al., 2017; Li et al., 2018; Rashid et al., 2011; Zhang
210 et al., 2020; Zorzi et al., 2015). Stalagmites in Mawmluh Cave record variations in river runoff in the surrounding area;
211 these variations are determined by the impacts of surface sea temperature (SST) and water vapor transport paths (Dutt et
212 al., 2015). In fact, the Mawmluh Cave records of the South Asian monsoon strength are driven by temperature gradients
213 that drive changes in winds and moisture transport into the BoB (Dutt et al., 2015), not just responding to the rainfall
214 amount. The smectite percentage changes measured in core 17I106 were slightly correlated after Heinrich event 1 (H1) but
215 were irrelevant before H1 (Figure 6b). This indicated that the combination of temperature and moisture failed to play a
216 crucial role in smectite transport to core 17I106, although weathering features in the source area may be shaped by the
217 South Asian monsoon. Moreover, the view could be confirmed by the smectite record obtained from the studied core not

218 being well correlated with records previously obtained in the Andaman Sea (Figure 6c, 6d, Gebregiorgis et al., 2016) or
219 with a sporopollen record obtained in Southwest China (Figure 6e, 6f, Zhang et al., 2020), especially before the LGM. The
220 consistency of salinity and SST in core SK 168 (Figure 6c, 6d) and moisture and temperature index (Figure 6e, 6f) in
221 Southwest China reveal that the hydroclimate in the South Asian monsoon region might have been influenced by SST in
222 the Indian Ocean. All these inconsistencies between the smectite percentage in core 17I106 and monsoon records indicate
223 that smectite supplementation may be mainly controlled by rainfall rather than by chemical weathering due to
224 thermodynamic differences between sea and land environments (Liu et al., 2020b).

225 During the late LGM, the smectite percentage increased abnormally in core 17I106, and this increase cannot be
226 explained by dry and cold weathering conditions, a lower sea level or a weakened summer monsoon at that time. In contrast,
227 this abnormal change may have been attributed to an increase in the smectite input in sediments from the Burman source
228 area or to a decrease in the amounts of sediment input from the Himalayas. Under the influence of the winter monsoon
229 during the LGM, the denuded sediments on the Irrawaddy estuary shelf may have been transported southward through the
230 west side of Andaman Island (Prajith et al., 2018), as was confirmed in previous work showing that the winter monsoon
231 led to an increase in terrestrial materials from the Irrawaddy River to the Ninetyeast Ridge during the Heinrich event
232 (Ahmad et al., 2005). However, the winter monsoon was strong in the western part of the study area from 21 to 15 ka
233 (Figure 6g), and the sea level remained relatively low during that period (Gautam et al., 2020). The smectite percentages
234 in the studied core increased significantly from 21 to 19 ka and dropped rapidly after 19 ka. This inconsistency contradicts
235 the conclusion that the increased smectite percentage in the source area was caused by a strong winter monsoon. Moreover,
236 the changes in the sediment compositions measured in the Himalayan source area were probably related to variations in
237 regional glaciers. During the LGM period, the increased glacial cover may have reduced surface runoff and further the
238 transport of physical weathering products, while the increased amount of ice meltwater may have transported more illites
239 following glacial melt. However, the reduced glacial area in the Himalayas during 18-15 ka did not occur simultaneously

240 with the increased illite percentage (Yan et al., 2020; Weldeab et al., 2019, Figure 6h). Therefore, the abnormal changes
241 measured in the smectite percentage during the late LGM period were caused by other climate-driven mechanisms, and the
242 millennium-scale smectite percentage fluctuations that occurred before the LGM require a more reasonable explanation.

243 **4.3. The ITCZ shift in the EIO**

244 Changes in rainfall and the corresponding runoff are generally utilized to explain short-term variations in clay minerals. In
245 the EIO, rainfall is controlled by monsoon activities (An et al., 2011; Beck et al., 2018; Gebregiorgis et al., 2016) and/or
246 ITCZ migrations (Deplazes et al., 2013; Stoll et al., 2007; Tan et al., 2019). Glacial-interglacial monsoon precipitation
247 changes at the regional scale are shaped by dynamics (changes in the wind fields) and temperature (McGee, 2020). The
248 wind fields may be driven by the relative dominance of the northern low-pressure and southern high-pressure systems (An
249 et al., 2011) and cross-equatorial moisture transport (Clemens et al., 2021), while the SST in the eastern Indian Ocean
250 (Zhang et al., 2020) or western Indian Ocean (Wang et al., 2022), surface and subsurface temperature changes (Tierney et
251 al., 2015), and temperature gradients (Weldeab et al., 2022) also play an important role in South Asian rainfall. At the same
252 time, as a climate-driving force in low-latitude regions, ITCZ migrations may be the main factor responsible for regional
253 hydrological changes (Deplazes et al., 2013; Weber et al., 2018) since the shift in the ITCZ was considered to control
254 rainfall distribution and intensity in central India over geological time scales (Zorzi et al., 2015) and to cause summer
255 temperature and moisture fluctuations in southwestern China during the last deglaciation (Zhang et al., 2019).

256 During the glacial-interglacial period, the ITCZ migrated north-south and balanced thermal differences by transferring
257 atmospheric heat; this process represents an indispensable climate-regulating power on Earth (Broccoli et al., 2006; McGee
258 et al., 2018; Schneider et al., 2014). In the Cariaco Basin and Arabian Seas (Figure 7a-b), tropical rainfall is highly
259 correlated with the North Atlantic climate, and sea ice variations in the North Atlantic affect the north-south shift of the
260 ITCZ in low-latitude regions through atmospheric circulation and ocean processes (Deplazes et al., 2013). The smectite
261 particles measured in core 17I106 mainly came from the Myanmar source area; in this area, rainfall is greatly affected by

262 the seasonal shift of the ITCZ. Before the LGM, the smectite percentages in the study core were well matched with the
263 ITCZ record in the Arabian Sea, where the supplementation of smectite percentages reached the peak when the ITCZ
264 shifted significantly northward (Figure 2b; Deplazes et al., 2013). During cold climate events, when the ITCZ moved
265 significantly southward, rainfall decreased, and the smectite percentages decreased correspondingly in the source area.
266 Therefore, we suggest that these changes in the smectite percentages in the studied core are correlated with ITCZ migration
267 and that rainfall is an important factor determining the smectite percentage from the source area of Myanmar on the
268 millennial scale. If precipitation induced by wind and temperature of the South Asian monsoon have an intense impact on
269 the source area, the source area monsoon indicators, for example, foraminifera, sporopollen, stalagmite (Figure 6) and other
270 indicators, would correspondingly change, but our record failed to catch these variations in monsoon indicators in the BoB.
271 We suggest that every factor affecting precipitation induced by wind and temperature of the South Asian monsoon, as
272 mentioned above, may have made it difficult to cause millennial-scale fluctuations similar to the ITCZ shift during the
273 MIS3 period. The South Asian monsoon is indeed the result of combined factors that may contribute to the heterogeneity
274 of monsoon rainfall in the BoB, which were also influenced by the north-south shift of the ITCZ. In core 171106, the
275 corresponding variations in the relatively high smectite percentages and the northward shift of the ITCZ indicate that the
276 northward movement of the ITCZ is the most important factor influencing the incremental changes in river sediment load
277 corresponding to the increased smectite percentages in the Myanmar region. Here we emphasize that the northward and
278 southward ITCZ shifts bring about rainfall increases and decreases relative to other rainfall forces. The changes in clay
279 minerals reflect changes in clay mineral supply in the source area, and it is that these relative increases and decreases in
280 rainfall lead to changes, which is a response to environmental changes. The sporopollen evidence suggested a cold and wet
281 period during MIS3 in Yunnan, China (Zhang et al., 2020), which may have been caused by the frequent northward
282 movement of the ITCZ during this period.

283 Although the changes in smectite percentages in the study area are associated with ITCZ shifts before the LGM, the

284 ITCZ shift in the Indo-Pacific warm pool (IPWP) was more “regional” than those in the Arabian Sea and the Cariaco Basin
285 (Deplazes et al., 2013). During the late LGM, when the ITCZ did not move extensively in the Arabian Sea, the ITCZ
286 gradually shifted northward in the IPWP from 21-18 ka (Figure 7d, Ayliffe et al., 2013). However, the smectite percentage
287 increased significantly in the study area, and we have excluded the possibility that the winter monsoon or meltwater
288 influenced these changes. Further comparisons with IPWP records reveal that the ITCZ changes agree well with the
289 smectite percentage variations during the late LGM, indicating that the northern migration of the ITCZ induced high
290 smectite percentages in core 17I106 (Figure 7c, d). These results suggest that the clay minerals of core 17I106 are
291 inextricably linked to ITCZ shifts on the millennial scale. In summary, our smectite record shows that before the LGM, the
292 ITCZ was in a relatively southerly position in the Myanmar area, while during the late LGM, the northward movement of
293 the ITCZ in the BoB led to increased rainfall in the Myanmar source area and an increased supply of smectite. At the same
294 time, the ITCZ was not significantly shifted in the Arabian Sea region either pre-LGM or post-LGM, which is what the
295 Arabian Sea record shows (Deplaze et al., 2013).

296 The smectite percentage in the studied core is different from the ITCZ records in some periods, such as the late LGM,
297 revealing that regional changes in the ITCZ were significantly obvious and that the ITCZ is not a simple N-S displacement.
298 This consistency may indicate that the regional extension of the north-south thermodynamic gradient in the EIO exceeded
299 that in the Arabian Sea and that the north-south shift of the ITCZ caused the climate systems of the Northern and Southern
300 Hemispheres to be more closely connected in the EIO during the late LGM (Huang et al., 2019; Zhuravleva et al., 2021).
301 A recent study considered less northward migration of the summer ITCZ position in the western BoB than in the eastern
302 BoB during Heinrich Stadials HS1 and HS5 (Ota et al., 2022), which indicated that regional ITCZ variations in the BoB
303 may be very common. These factors may be correlated with observed variations in regional air-sea interactions, such as
304 the exposure of the Sunda Shelf (DiNezio and Tierney, 2013), the effect of the thermocline in the EIO (Mohtadi et al., 2017)
305 and even potential El Nino-like mode (Thirumalai et al., 2019) and IOD (Abram et al., 2020) changes, which may make

306 the ITCZ shift more dramatic or keep the ITCZ position in the Northern Hemisphere longer. Thus, the regional variations
307 in the ITCZ should be fully considered when studying climate change, especially in low-latitude regions that are sensitive
308 to climatic and environmental changes, such as the EIO (Niedermeyer et al., 2014).

309 **5. Conclusion**

310 We reconstructed the variations in sediment sources on the Ninetyeast Ridge over the past 45 ka. The main source areas
311 comprise the Himalayas transported by the G-B River and Irrawaddy River; sediments were stably supplied from these
312 regions throughout the studied core. When North Atlantic cold events (Heinrich and YD) occurred, chemical weathering
313 weakened and physical weathering increased; correspondingly, the smectite percentage decreased and the illite percentage
314 increased. From 35-21 ka, the falling sea level led to an increase in the exposed area of the Andaman and Nicobar Islands
315 and further hindered the entrance of smectite from the Andaman Sea into the study area. At the same time, the influence of
316 the South Asian monsoon on the sediment supply was not obvious. The time-phase mismatches observed among records
317 excluded the influence of Burman shelf sediment erosion forced by the winter monsoon or of variations in G-B river
318 sediments induced by ice meltwater on the abnormal increases observed in the smectite percentages during the late LGM.
319 The smectite record of core 17I106 is consistent with the ITCZ changes recorded on the millennial scale, indicating that
320 the ITCZ controls the rainfall in the Burman source area and, further, the clay mineral variations in the study area. The
321 inferred ITCZ shift recorded in the studied core coincided with the global ITCZ change that occurred before the LGM, but
322 during the late LGM, the core record was consistent with the change in the regional ITCZ recorded by the IPWP. This
323 revealed that regional changes in the ITCZ were very significant, and the ITCZ is not a simple N-S displacement at the
324 same time. Thus, the regional variations in the ITCZ should be fully considered when studying climate change, especially
325 in low-latitude regions that are sensitive to climate and environmental changes.

326 **Author contributions.**

327 J.L. and Y.H. conceived and designed the experiment. X.X. wrote the manuscript with contributions from all authors. L.Z.
328 and L.Y. provided the ages of planktonic foraminifera, and S.L., Y.Y., L.C., and L.T. helped to analyze the measured data
329 and discuss the related relevant topics in this manuscript.

330 **Competing interests.**

331 The authors declare that they have no conflicts of interest.

332 **Acknowledgements.**

333 We thank Hui Zhang for the help of Sr-Nd isotope measurements. We also thank the editor Pierre Francus, Prof. Michael
334 E. Weber and another anonymous reviewer for their constructive comments. Core sediment samples were collected onboard
335 of *R/V "Shiyan 1"* implementing the open research cruise NORC 2012-08 supported by the NSFC Shiptime Sharing Project.

336 **Financial support.**

337 This work has been jointly funded by the National Natural Science Foundation of China (42176075, 42130412 and
338 41576044), Key Special Project for Introduced Talents Team of Southern Marine Science and Engineering Guangdong
339 Laboratory (Guangzhou) (GML2019ZD0206), and the Open Fund of the Key Laboratory of Submarine Geosciences,
340 Ministry of Natural Resources (KLSG2102).

341 **Data Availability Statement.**

342 All dataset is available on Science Data Bank
343 (<https://www.scidb.cn/detail?dataSetId=55c7dcf1f8344c658099dfe030264b2f>).

344 **References**

345 Abram, N.J., Hargreaves, J.A., Wright, N.M., Thirumalai, K., Ummenhofer, C.C., and England, M.H.: Palaeoclimate
346 perspectives on the Indian Ocean Dipole, *Quat. Sci. Rev.*, 237, 106302,

347 <https://doi.org/10.1016/j.quascirev.2020.106302>, 2020.

348 Ahmad, S.M., Anil Babu, G., Padmakumari, V.M., Dayal, A.M., Sukhija, B.S., and Nagabhushanam, P.: Sr, Nd isotopic
349 evidence of terrigenous flux variations in the Bay of Bengal: Implications of monsoons during the last ~34,000 years,
350 *Geophys. Res. Lett.*, 32, L22711, <https://doi.org/10.1029/2005GL024519>, 2005.

351 Ahmad, S.M., Padmakumari, V.M. and Babu, G.A.: Strontium and neodymium isotopic compositions in sediments from
352 Godavari, Krishna and Pennar rivers, *Curr. Sci.*, 97, 1766-1769, 2009.

353 Ali, S., Hathorne, E.C., Frank, M., Gebregiorgis, D., Statterger, K., Stumpf, R., Kutterolf, S., Johnson, J.E., and Giosan,
354 L.: South Asian monsoon history over the past 60 kyr recorded by radiogenic isotopes and clay mineral assemblages
355 in the Andaman Sea, *Geochem., Geophys., Geosy.*, 16, 505-521, <https://doi.org/10.1002/2014gc005586>, 2015.

356 Ali, S., Hathorne, E.C., and Frank, M.: Persistent Provenance of South Asian Monsoon-Induced Silicate Weathering Over
357 the Past 27 Million Years, *Paleoceanogr. Paleocl.*, 36, e2020PA003909, <https://doi.org/10.1029/2020PA003909>, 2021.

358 An, Z., Clemens, S., Shen, J., Qiang, X., Jin, Z., Sun, Y., Prell, W., Luo, J., Wang, S., Xu, H., Cai, Y., Zhou, W., Liu, X.,
359 Liu, W., Shi, Z., Yan, L., Xiao, X., Chang, H., Wu, F., Ai, L., and Lu, F.: Glacial-Interglacial Indian Summer Monsoon
360 Dynamics, *Science*, 333, 719-723, <https://doi.org/10.1126/science.1203752>, 2011.

361 Awasthi, N., Ray, J.S., Singh, A.K., Band, S.T., and Rai, V.K.: Provenance of the Late Quaternary sediments in the Andaman
362 Sea: Implications for monsoon variability and ocean circulation, *Geochem., Geophys., Geosy.*, 15, 3890-3906,
363 <https://doi.org/10.1002/2014gc005462>, 2014.

364 Ayliffe, L.K., Gagan, M.K., Zhao, J.X., Drysdale, R.N., Hellstrom, J.C., Hantoro, W.S., Griffiths, M.L., Scott-Gagan, H.,
365 Pierre, E.S., Cowley, J.A., and Suwargadi, B.W.: Rapid interhemispheric climate links via the Australasian monsoon
366 during the last deglaciation, *Nat. Commun.*, 4, 2908, <https://doi.org/10.1038/ncomms3908>, 2013.

367 Beck, J.W., Zhou, W., Li, C., Wu, Z., White, L., Xian, F., Kong, X.H., and An, Z.: A 550,000-year record of East Asian
368 monsoon rainfall from Be-10 in loess, *Science*, 360, 877-881, <https://doi.org/10.1126/science.aam5825>, 2018.

369 Bejugam, P., and Nayak, G.N.: Source and depositional processes of the surface sediments and their implications on
370 productivity in recent past off Mahanadi to Pennar River mouths, western Bay of Bengal, *Palaeogeogr.*,
371 *Palaeoclimatol.*, *Palaeoecol.*, 483, 58-69, <https://doi.org/10.1016/j.palaeo.2016.12.006>, 2017.

372 Biscaye, P.E.: Mineralogy and sedimentation of recent deep-sea clay in Atlantic Ocean and adjacent seas and oceans, *Geol.*
373 *Soc. Amer. Bull.*, 76, 803-832, [https://doi.org/10.1130/0016-7606\(1965\)76\[803:masord\]2.0.co;2](https://doi.org/10.1130/0016-7606(1965)76[803:masord]2.0.co;2), 1965.

374 Blaauw, M., and Christen, J.A.: Flexible Paleoclimate Age-Depth Models Using an Autoregressive Gamma Process,
375 *Bayesian Analysis*, 6, 457-474, <https://doi.org/10.1214/11-ba618>, 2011.

376 Broccoli, A.J., Dahl, K.A., and Stouffer, R.J.: Response of the ITCZ to Northern Hemisphere cooling, *Geophys. Res. Lett.*,
377 33, L01702, <https://doi.org/10.1029/2005GL024546>, 2006.

378 Chamley, H.: *Clay Sedimentology*, Springer, Berlin, 623 pp., 1989.

379 Chatterjee, A., Shankar, D., McCreary, J.P., Vinayachandran, P.N., and Mukherjee, A.: Dynamics of Andaman Sea
380 circulation and its role in connecting the equatorial Indian Ocean to the Bay of Bengal, *J. Geophys. Res. Oceans*, 122,
381 3200-3218, <https://doi.org/10.1002/2016JC012300>, 2017.

382 Clemens, S.C., Yamamoto, M., Thirumalai, K., Giosan, L., Richey, J.N., Nilsson-Kerr, K., Rosenthal, Y., Anand, P.,
383 McGrath, S.M.: Remote and local drivers of Pleistocene South Asian summer monsoon precipitation: A test for future
384 predictions. *Sci. Adv.*, 7(23), eabg3848. <https://doi.org/10.1126/sciadv.abg3848>, 2021.

385 Colin, C., Turpin, L., Bertaux, J., Desprairies, A., and Kissel, C.: Erosional history of the Himalayan and Burman Ranges
386 during the last two glacial-interglacial cycles, *Earth Planet. Sci. Lett.*, 171, 647-660, [https://doi.org/10.1016/S0012-](https://doi.org/10.1016/S0012-821X(99)00184-3)
387 [821X\(99\)00184-3](https://doi.org/10.1016/S0012-821X(99)00184-3), 1999.

388 Colin, C., Turpin, L., Blamart, D., Frank, N., Kissel, C., and Duchamp, S.: Evolution of weathering patterns in the Indo-
389 Burman Ranges over the last 280 kyr: Effects of sediment provenance on $^{87}\text{Sr}/^{86}\text{Sr}$ ratios tracer, *Geochem., Geophys.*,
390 *Geosy.*, 7, Q03007, <https://doi.org/10.1029/2005gc000962>, 2006.

391 Curray, J.R., Emmel, F.J., and Moore, D.G.: The Bengal Fan: morphology, geometry, stratigraphy, history and processes,
392 Mar. Petrol. Geol., 19, 1191-1223, [https://doi.org/10.1016/S0264-8172\(03\)00035-7](https://doi.org/10.1016/S0264-8172(03)00035-7), 2003.

393 Deplazes, G., Lückge, A., Peterson, L.C., Timmermann, A., Hamann, Y., Hughen, K.A., Röhl, U., Laj, C., Cane, M.A.,
394 Sigman, D.M., and Haug, G.H.: Links between tropical rainfall and North Atlantic climate during the last glacial
395 period, Nat. Geosci., 6, 213-217, <https://doi.org/10.1038/ngeo1712>, 2013.

396 DiNezio, P.N., and Tierney, J.E.: The effect of sea level on glacial Indo-Pacific climate, Nat. Geosci., 6, 485-491,
397 <https://doi.org/10.1038/ngeo1823>, 2013.

398 Dou, Y., Yang, S., Shi, X., Clift, P.D., Liu, S., Liu, J., Li, C., Bi, L., and Zhao, Y.: Provenance weathering and erosion
399 records in southern Okinawa Trough sediments since 28 ka: Geochemical and Sr–Nd–Pb isotopic evidences, Chem.
400 Geol., 425, 93-109. <https://doi.org/10.1016/j.chemgeo.2016.01.029>, 2016.

401 Dutt, S., Gupta, A.K., Clemens, S.C., Cheng, H., Singh, R.K., Kathayat, G., and Edwards, R.L.: Abrupt changes in Indian
402 summer monsoon strength during 33,800 to 5500 years B.P., Geophys. Res. Lett., 42, 5526-5532,
403 <https://doi.org/10.1002/2015gl064015>, 2015.

404 Erosion, H.S.: Sedimentation and sedimentary origin of clays, in: Velde, B. (Ed.), Origin and Mineralogy of Clays. Clays
405 Environment., Springer, Berlin, pp. 162-219, 1995.

406 Fournier, L., Fauquembergue, K., Zaragosi, S., Zorzi, C., Malaize, B., Bassinot, F., Joussain, R., Colin, C., Moreno, E., and
407 Leparmentier, F.: The Bengal fan: external controls on the Holocene Active Channel turbidite activity, Holocene, 27
408 (6), 900-913, <https://doi.org/10.1177/0959683616675938>, 2017.

409 Gautam, P.K., Narayana, A.C., Kumar, P.K., Bhavani, P.G., Yadava, M.G., and Jull, A.J.T.: Indian monsoon variability
410 during the last 46 kyr: isotopic records of planktic foraminifera from southwestern Bay of Bengal, J. Quat. Sci., 36,
411 138-151, <https://doi.org/10.1002/jqs.3263>, 2020.

412 Gebregiorgis, D., Hathorne, E.C., Sijinkumar, A.V., Nath, B.N., Nürnberg, D., and Frank, M.: South Asian summer

413 monsoon variability during the last ~54 kyrs inferred from surface water salinity and river runoff proxies, *Quat. Sci.*
414 *Rev.*, 138, 6-15, <https://doi.org/10.1016/j.quascirev.2016.02.012>, 2016.

415 Gibbs, R.J.: Clay mineral segregation in the marine environment, *J. Sediment. Res.*, 47, 237-243, 1977.

416 Goodbred, S.L., and Kuehl, S.A.: Enormous Ganges-Brahmaputra sediment discharge during strengthened early Holocene
417 monsoon, *Geology*, 28, 1083-1086, [https://doi.org/10.1130/0091-7613\(2000\)028<1083:Egbsdd>2.3.Co;2](https://doi.org/10.1130/0091-7613(2000)028<1083:Egbsdd>2.3.Co;2), 2000.

418 Grant, K.M., Rohling, E.J., Ramsey, C.B., Cheng, H., Edwards, R.L., Florindo, F., Heslop, D., Marra, F., Roberts, A.P.,
419 Tamisiea, M.E., and Williams, F.: Sea-level variability over five glacial cycles, *Nat. Commun.*, 5, 5076,
420 <https://doi.org/10.1038/ncomms6076>, 2014.

421 Hanebuth, T., Stattegger, K., and Grootes, P.M.: Rapid Flooding of the Sunda Shelf: A Late-Glacial Sea-Level Record,
422 *Science*, 288, 1033-1035, <https://doi.org/10.1126/science.288.5468.1033>, 2000.

423 Huang, J., Wan, S., Li, A., and Li, T.: Two-phase structure of tropical hydroclimate during Heinrich Stadial 1 and its global
424 implications, *Quat. Sci. Rev.*, 222, 105900, <https://doi.org/10.1016/j.quascirev.2019.105900>, 2019.

425 Jacobsen, S.B. and Wasserburg, G.J.: Sm-Nd isotopic evolution of chondrites, *Earth Planet. Sci. Lett.*, 50, 139-155,
426 [https://doi.org/10.1016/0012-821x\(80\)90125-9](https://doi.org/10.1016/0012-821x(80)90125-9), 1980.

427 Jousain, R., Colin, C., Liu, Z., Meynadier, L., Fournier, L., Fauquembergue, K., Zaragosi, S., Schmidt, F., Rojas, V., and
428 Bassinot, F.: Climatic control of sediment transport from the Himalayas to the proximal NE Bengal Fan during the
429 last glacial-interglacial cycle, *Quat. Sci. Rev.*, 148, 1-16, <https://doi.org/10.1016/j.quascirev.2016.06.016>, 2016.

430 Jousain, R., Liu, Z., Colin, C., Duchamp-Alphonse, S., Yu, Z., Moréno, E., Fournier, L., Zaragosi, S., Dapigny, A.,
431 Meynadier, L., and Bassinot, F.: Link between Indian monsoon rainfall and physical erosion in the Himalayan system
432 during the Holocene, *Geochem., Geophys., Geosy.*, 18, 3452-3469, <https://doi.org/10.1002/2016gc006762>, 2017.

433 Kessarkar, P.M., Rao, V.P., Ahmad, S.M., Patil, S.K., Kumar, A.A., Babu, G.A., Chakraborty, S., and Rajan, R.S.: Changing
434 sedimentary environment during the Late Quaternary: Sedimentological and isotopic evidence from the distal Bengal

435 Fan, Deep Sea Res. Pt I: Oceanogr. Res. Papers, 52, 1591-1615, <https://doi.org/10.1016/j.dsr.2005.01.009>, 2005.

436 Khan, M.H.R., Liu, J., Liu, S., Seddique, A.A., Cao, L., and Rahman, A.: Clay mineral compositions in surface sediments
437 of the Ganges-Brahmaputra-Meghna river system of Bengal Basin, Bangladesh, Mar. Geol., 412, 27-36,
438 <https://doi.org/10.1016/j.margeo.2019.03.007>, 2019.

439 Li, J., Liu, S., Shi, X., Feng, X., Fang, X., Cao, P., Sun, X.Q., Ye, W.X., Khokiattiwong, S., and Kornkanitnan, N.:
440 Distributions of clay minerals in surface sediments of the middle Bay of Bengal: Source and transport pattern,
441 Continent. Shelf Res., 145, 59-67, <https://doi.org/10.1016/j.csr.2017.06.017>, 2017.

442 Li, J., Liu, S., Shi, X., Zhang, H., Fang, X., Chen, M.-T., Cao, P., Sun, X. Q., Ye, W.X., Wu, K.K., Khokiattiwong, S., and
443 Kornkanitnan, N.: Clay minerals and Sr-Nd isotopic composition of the Bay of Bengal sediments: Implications for
444 sediment provenance and climate control since 40 ka, Quat. Internat., 493, 50-58,
445 <https://doi.org/10.1016/j.quaint.2018.06.044>, 2018.

446 Licht, A. France-Lanord, C., Reisberg, L., Fontaine, C., Soe, A.N., and Jaeger, J.J.: A palaeo Tibet-Myanmar connection?
447 Reconstructing the Late Eocene drainage system of central Myanmar using a multi-proxy approach, J. Geol. Soc.,
448 170, 929-939, <https://doi.org/10.1144/jgs2012-126>, 2013.

449 Liu, J., He, W., Cao, L., Zhu, Z., Xiang, R., Li, T., Shi, X., and Liu, S.: Staged fine-grained sediment supply from the
450 Himalayas to the Bengal Fan in response to climate change over the past 50,000 years, Quat. Sci. Rev., 212, 164-177,
451 <https://doi.org/10.1016/j.quascirev.2019.04.008>, 2019.

452 Liu, J P., Kuehl, S.A., Pierce, A.C., Williams, J., Blair, N.E., Harris, C., Aung, D.W., and Aye, Y.Y.: Fate of Ayeyarwady
453 and Thanlwin Rivers Sediments in the Andaman Sea and Bay of Bengal, Mar. Geol., 423, 106137,
454 <https://doi.org/10.1016/j.margeo.2020.106137>, 2020a.

455 Liu, S., Li, J., Zhang, H., Cao, P., Mi, B., Khokiattiwong, S., Kornkanitnan, N., and Shi, X.: Complex response of
456 weathering intensity registered in the Andaman Sea sediments to the Indian Summer Monsoon over the last 40 kyr,

457 Mar. Geol., 426, 106206, <https://doi.org/10.1016/j.margeo.2020.106206>, 2020b.

458 Liu, S., Ye, W., Cao, P., Zhang, H., Chen, M. -T., Li, X., Li, J., Pan, H.-J., Khokiattiwong, S., Kornkanitnan, N., and Shi,
459 X.: Paleoclimatic responses in the tropical Indian Ocean to regional monsoon and global climate change over the last
460 42 kyr, Mar. Geol., 438, 106542, <https://doi.org/10.1016/j.margeo.2021.106542>, 2021.

461 Liu, Z., Wang, H., Hantoro, W. S., Sathiamurthy, E., Colin, C., Zhao, Y., Li, J.: Climatic and tectonic controls on chemical
462 weathering in tropical Southeast Asia (Malay Peninsula, Borneo, and Sumatra), Chem. Geol., 291, 1-12,
463 <https://doi.org/10.1016/j.chemgeo.2011.11.015>, 2012.

464 Lupker, M., France-Lanord, C., Galy, V., Lavé, J., and Kudrass, H.: Increasing chemical weathering in the Himalayan
465 system since the Last Glacial Maximum, Earth Planet. Sci. Lett., 365, 243-252,
466 <https://doi.org/10.1016/j.epsl.2013.01.038>, 2013.

467 Marzin, C., Kallel, N., Kageyama, M., Duplessy, J.C., and Braconnot, P.: Glacial fluctuations of the Indian monsoon and
468 their relationship with North Atlantic climate: new data and modelling experiments, Clim. Past., 9, 2135-2151,
469 <https://doi.org/10.5194/cp-9-2135-2013>, 2013.

470 McGee, D., Moreno-Chamarro, E., Green, B., Marshall, J., Galbraith, E., and Bradtmiller, L.: Hemispherically asymmetric
471 trade wind changes as signatures of past ITCZ shifts, Quat. Sci. Rev., 180, 214-228,
472 <https://doi.org/10.1016/j.quascirev.2017.11.020>, 2018.

473 McGee, D.: Glacial-Interglacial Precipitation Changes. Ann. Rev. Mar. Sci., 12, 525-557. [https://doi.org/10.1146/annurev-](https://doi.org/10.1146/annurev-marine-010419-010859)
474 [marine-010419-010859](https://doi.org/10.1146/annurev-marine-010419-010859), 2020.

475 Mohtadi, M., Prange, M., Oppo, D. W., De Pol-Holz, R., Merkel, U., Zhang, X., Steinke, S., and Luckge, A.: North Atlantic
476 forcing of tropical Indian Ocean climate, Nature, 509, 76-80, <https://doi.org/10.1038/nature13196>, 2014.

477 Mohtadi, M., Prange, M., Steinke, S.: Palaeoclimatic insights into forcing and response of monsoon rainfall, Nature, 533,
478 191-199, <https://doi.org/10.1038/nature17450>, 2016.

479 Mohtadi, M., Prange, M., Schefuss, E., and Jennerjahn, T.C.: Late Holocene slowdown of the Indian Ocean Walker
480 circulation, *Nat. Commun.*, 8, 1015, <https://doi.org/10.1038/s41467-017-00855-3>, 2017.

481 Niedermeyer, E.M., Sessions, A.L., Feakins, S.J., and Mohtadi, M.: Hydroclimate of the western Indo-Pacific Warm Pool
482 during the past 24,000 years, *P. Natl. Acad. Sci. USA*, 111, 9402-9406, <https://doi.org/10.1073/pnas.1323585111>, 2014.

483 Ota, Y., Kawahata, H., Kuroda, J., Suzuki, A., Abe-Ouchi, A., and Jimenez-Espejo, F.J.: Millennial-scale variability of
484 Indian summer monsoon constrained by the western Bay of Bengal sediments: Implication from geochemical proxies
485 of sea surface salinity and river runoff, *Glob. Planet. Change*, 208, <https://doi.org/10.1016/j.gloplacha.2021.103719>,
486 2022.

487 Peng, J., Yang, X., Toney, J.L., Ruan, J., Li, G., Zhou, Q., Gao, H., Xie, Y., Chen, Q., and Zhang, T.: Indian Summer
488 Monsoon variations and competing influences between hemispheres since ~35 ka recorded in Tengchongqinghai Lake,
489 southwestern China, *Palaeogeogr., Palaeoclimatol., Palaeoecol.*, 516, 113-125,
490 <https://doi.org/10.1016/j.palaeo.2018.11.040>, 2019.

491 Prajith, A., Tyagi, A., and John Kurian, P.: Changing sediment sources in the Bay of Bengal: Evidence of summer monsoon
492 intensification and ice-melt over Himalaya during the Late Quaternary, *Palaeogeogr., Palaeoclimatol., Palaeoecol.*,
493 511, 309-318, <https://doi.org/10.1016/j.palaeo.2018.08.016>, 2018.

494 Rashid, H., England, E., Thompson, L., and Polyak, L.: Late Glacial to Holocene Indian Summer Monsoon Variability
495 Based upon Sediment Records Taken from the Bay of Bengal, *Terr., Atmosp. Ocean. Sci.*, 22, 215-228,
496 [https://doi.org/10.3319/TAO.2010.09.17.02\(TibXS\)](https://doi.org/10.3319/TAO.2010.09.17.02(TibXS)), 2011.

497 Rayaroth, M.K., Peter, B.N., and Mahmud, M.R.: High-resolution surface circulation of the Bay of Bengal derived from
498 satellite observation data, *J. Mar. Sci. Technol.*, 24, 656-668, <https://doi.org/10.6119/JMST-015-1215-2>, 2016.

499 Raza, T., and Ahmad, S.M.: Surface and deep water variations in the northeast Indian Ocean during 34-6 ka BP: evidence
500 from carbon and oxygen isotopes of fossil foraminifera, *Quat. Internat.*, 298, 37-44,

501 <https://doi.org/10.1016/j.quaint.2012.05.005>, 2013.

502 Reimer, P.J., Austin, W.E.N., Bard, E., Bayliss, A., Blackwell, P.G., Bronk Ramsey, C., Butzin, M., Cheng, H., Edwards,
503 R.L., Friedrich, M., Grootes, P.M., Guilderson, T.P., Hajdas, I., Heaton, T.J., Hogg, A.G., Hughen, K.A., Kromer, B.,
504 Manning, S.W., Muscheler, R., Palmer, J.G., Pearson, C., van der Plicht, J., Reimer, R.W., Richards, D.A., Scott, E.M.,
505 Southon, J.R., Turney, C.S.M., Wacker, L., Adolphi, F., Büntgen, U., Capano, M., Fahrni, S.M., Fogtmann-Schulz, A.,
506 Friedrich, R., Köhler, P., Kudsk, S., Miyake, F., Olsen, J., Reinig, F., Sakamoto, M., Sookdeo, A., and Talamo, S.: The
507 intcal20 northern hemisphere radiocarbon age calibration curve (0-55 cal kBP), *Radiocarbon*, 62, 725-757,
508 <https://doi.org/10.1017/RDC.2020.41>, 2020.

509 Rodolfo, K.S.: Sediments of Andaman Basin, northeastern Indian Ocean, *Mar. Geol.*, 7, 371-380,
510 [https://doi.org/10.1016/0025-3227\(69\)90014-0](https://doi.org/10.1016/0025-3227(69)90014-0), 1969.

511 Schneider, T., Bischoff, T., and Haug, G.H.: Migrations and dynamics of the intertropical convergence zone, *Nature*, 513,
512 45-53, <https://doi.org/10.1038/nature13636>, 2014.

513 Schott, F.A., and McCreary, J.P.: The monsoon circulation of the Indian Ocean, *Progr. Oceanogr.*, 51, 1-123,
514 [https://doi.org/10.1016/s0079-6611\(01\)00083-0](https://doi.org/10.1016/s0079-6611(01)00083-0), 2001.

515 Seo, I., Khim, B.-K., Cho, H.G., Huh, Y., Lee, J., and Hyeong, K.: Origin of the Holocene Sediments in the Ninetyeast
516 Ridge of the Equatorial Indian Ocean, *Ocean Sci. J.*, <https://doi.org/10.1007/s12601-021-00052-w>, 2022.

517 Shankar, D., Vinayachandran, P.N., and Unnikrishnan, A.S.: The monsoon currents in the north Indian Ocean, *Progr.*
518 *Oceanogr.*, 52, 63-120, [https://doi.org/10.1016/s0079-6611\(02\)00024-1](https://doi.org/10.1016/s0079-6611(02)00024-1), 2002.

519 Stoll, H. M., Vance, D., and Arevalos, A.: Records of the Nd isotope composition of seawater from the Bay of Bengal:
520 Implications for the impact of Northern Hemisphere cooling on ITCZ movement, *Earth Planet. Sci. Lett.*, 255, 213-
521 228, <https://doi.org/10.1016/j.epsl.2006.12.016>, 2007.

522 Sun, Y., Clemens, S.C., Morrill, C., Lin, X., Wang, X., and An, Z.: Influence of Atlantic meridional overturning circulation

523 on the East Asian winter monsoon, *Nat. Geosci.*, 5, 46-49. <https://doi.org/10.1038/ngeo1326>, 2011.

524 Svensson, A., Andersen, K.K., Bigler, M., Clausen, H.B., Dahl-Jensen, D., Davies, S.M., Johnsen, S.J., Muscheler, R.,
525 Parrenin, F., Rasmussen, S.O., Röthlisberger, R., Seierstad, I., Steffensen, J.P., and Vinther, B.M.: A 60 000 year
526 Greenland stratigraphic ice core chronology, *Clim. Past*, 4, 47-57, <https://doi.org/10.5194/cp-4-47-2008>, 2008.

527 Tan, L., Shen, C.C., Lowemark, L., Chawchai, S., Edwards, R.L., Cai, Y., Breitenbach, S.F.M., Cheng, H., Chou, Y.C.,
528 Duerrast, H., Partin, J.W., Cai, W., Chabangborn, A., Gao, Y., Kwiecien, O., Wu, C.C., Shi, Z., Hsu, H.H., and
529 Wohlfarth, B.: Rainfall variations in central Indo-Pacific over the past 2,700 y, *P. Nation. Acad. Sci. USA*, 116, 17201-
530 17206, <https://doi.org/10.1073/pnas.1903167116>, 2019.

531 Thompson, W.G., and Goldstein, S.L.: A radiometric calibration of the SPECMAP timescale, *Quat. Sci. Rev.*, 25, 3207-
532 3215, <https://doi.org/10.1016/j.quascirev.2006.02.007>, 2006.

533 Thirumalai, K., DiNezio, P.N., Tierney, J.E., Puy, M., Mohtadi, M.: An El Niño Mode in the Glacial Indian Ocean?
534 *Paleoceanogr. Paleoclimatol.*, 34, 1316-1327, <https://doi.org/10.1029/2019pa003669>, 2019.

535 Tierney, J.E., Pausata, F.S.R., and deMenocal, P.: Deglacial Indian monsoon failure and North Atlantic stadials linked by
536 Indian Ocean surface cooling, *Nat. Geosci.*, 9, 46-50. <https://doi.org/10.1038/ngeo2603>, 2015.

537 Tripathy, G.R., Singh, S.K., and Bhushan, R.: Sr-Nd isotope composition of the Bay of Bengal sediment: Impact of climate
538 on erosion in the Himalaya, *Geochem. J.*, 45, 175-186, 2011.

539 Tripathy, G.R., Singh, S.K., and Ramaswamy, V.: Major and trace element geochemistry of Bay of Bengal sediments:
540 Implications to provenances and their controlling factors, *Palaeogeogr., Palaeoclimatol., Palaeoecol.*, 397, 20-30,
541 <https://doi.org/10.1016/j.palaeo.2013.04.012>, 2014.

542 Turner, S., and Foden, J.: U, Th and Ra disequilibria, Sr, Nd and Pb isotope and trace element variations in Sunda arc lavas:
543 predominance of a subducted sediment component, *Contr. Mineral. Petrol.*, 142, 43-57,
544 <https://doi.org/10.1007/s004100100271>, 2001.

545 Waelbroecka, C., Labeyrieab, L., Michela, E., Duplessya, J.C., McManusc, J.F., Lambeckd, K., Balbona, E., and
546 Labracherie, M.: Sea-level and deep water temperature changes derived from benthic foraminifera isotopic records,
547 *Quat. Sci. Rev.*, 21, 295-305, [https://doi.org/10.1016/s0277-3791\(01\)00101-9](https://doi.org/10.1016/s0277-3791(01)00101-9), 2002.

548 Wang, Y.V., Larsen, T., Lauterbach, S., Andersen, N., Blanz, T., Krebs-Kanzow, Gierz, P., and Schneider, R.R.: Higher sea
549 surface temperature in the Indian Ocean during the Last Interglacial weakened the South Asian monsoon, *P. Natl.*
550 *Acad. Sci. USA*, 119, e2107720119. <https://doi.org/10.1073/pnas.2107720119>, 2022.

551 Weber, M.E., Lantzsch, H., Dekens, P., Das, S.K., Reilly, B.T., Martos, Y.M., Meyer-Jacob, C., Agrahari, S., Ekblad, A.,
552 Titschack, J., Holmes, B., and Wolfgramm, P.: 200,000 years of monsoonal history recorded on the lower Bengal Fan
553 - strong response to insolation forcing, *Glob. Planet. Change*, 166, 107-119,
554 <https://doi.org/10.1016/j.gloplacha.2018.04.003>, 2018.

555 Weldeab, S., Rühlemann, C., Bookhagen, B., Pausata, F.S.R., and Perez - Lua, F.M.: Enhanced Himalayan Glacial Melting
556 During YD and H1 Recorded in the Northern Bay of Bengal, *Geochem., Geophys., Geosy.*, 20, 2449-2461,
557 <https://doi.org/10.1029/2018GC008065>, 2019.

558 Weldeab, S., Rühlemann, C., Ding, Q., Khon, V., Schneider, B., and Gray, W.R.: Impact of Indian Ocean surface
559 temperature gradient reversals on the Indian Summer Monsoon, *Earth Planet. Sci. Lett.*, 578, 117327,
560 <https://doi.org/10.1016/j.epsl.2021.117327>, 2022.

561 Winkler, A., Wolf-Welling, T., Stattegger, K., and Thiede, J.: Clay mineral sedimentation in high northern latitude deep-
562 sea basins since the Middle Miocene (ODP Leg 151, NAAG), *Interna. J. Earth Sci.*, 91 (1), 133–148,
563 <https://doi.org/10.1007/s005310100199>, 2002.

564 Yan, Q., Owen, L.A., Zhang, Z., Jiang, N., and Zhang, R.: Deciphering the evolution and forcing mechanisms of glaciation
565 over the Himalayan-Tibetan orogen during the past 20,000 years, *Earth Planet. Sci. Lett.*, 541, 116295,
566 <https://doi.org/10.1016/j.epsl.2020.116295>, 2020.

567 Ye, W., Liu, S., Fan, D., Zhang, H., Cao, P., Pan, H. -J., Li, J., Li, X., Fang, X., Khokiattiwong, S., Kornkanitnan, N., and
568 Shi, X.: Evolution of sediment provenances and transport processes in the central Bay of Bengal since the Last Glacial
569 Maximum, *Quat. Internat.*, (in press). <https://doi.org/10.1016/j.quaint.2020.12.007>, 2020.

570 Yu, Z., Colin, C., Wan, S., Saraswat, R., Song, L., Xu, Z., Clift, P., Lu, H., Lyle, M., Kulhanek, D., Hahn, A., Tiwari, M.,
571 Mishra, R., Miska, S., and Kumar, A.: Sea level-controlled sediment transport to the eastern Arabian Sea over the past
572 600 kyr: clay minerals and Sr-Nd isotopic evidence from IOD site U1457, *Quat. Sci. Rev.*, 205, 22-34,
573 <https://doi.org/10.1016/j.quascirev.2018.12.006>, 2019.

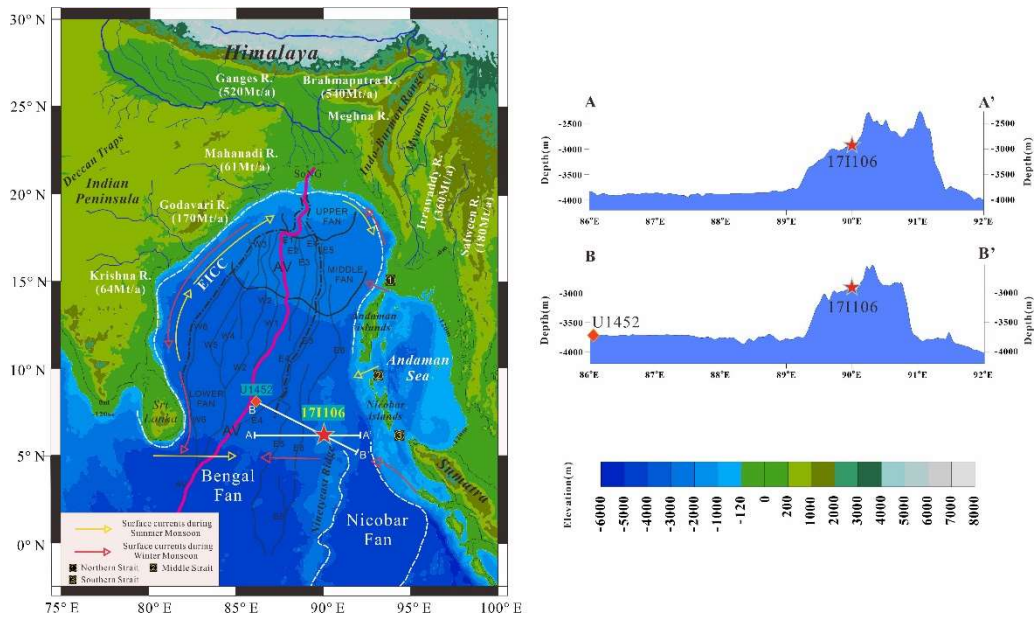
574 Zhang, E., Chang, J., Shulmeister, J., Langdon, P., Sun, W., Cao, Y., Yang, X., and Shen, J.: Summer temperature
575 fluctuations in Southwestern China during the end of the LGM and the last deglaciation, *Earth Planet. Sci. Lett.*, 509,
576 78-87, <https://doi.org/10.1016/j.epsl.2018.12.024>, 2019.

577 Zhang, X., Zheng, Z., Huang, K., Yang, X., and Tian, L.: Sensitivity of altitudinal vegetation in southwest China to changes
578 in the Indian summer monsoon during the past 68000 years, *Quat. Sci. Rev.*, 239, 106359,
579 <https://doi.org/10.1016/j.quascirev.2020.106359>, 2020.

580 Zhuravleva, A., Hüls, M., Tiedemann, R., and Bauch, H. A.: A 125-ka record of northern South American precipitation and
581 the role of high-to-low latitude teleconnections, *Quat. Sci. Rev.*, 270, 107159,
582 <https://doi.org/10.1016/j.quascirev.2021.107159>, 2021.

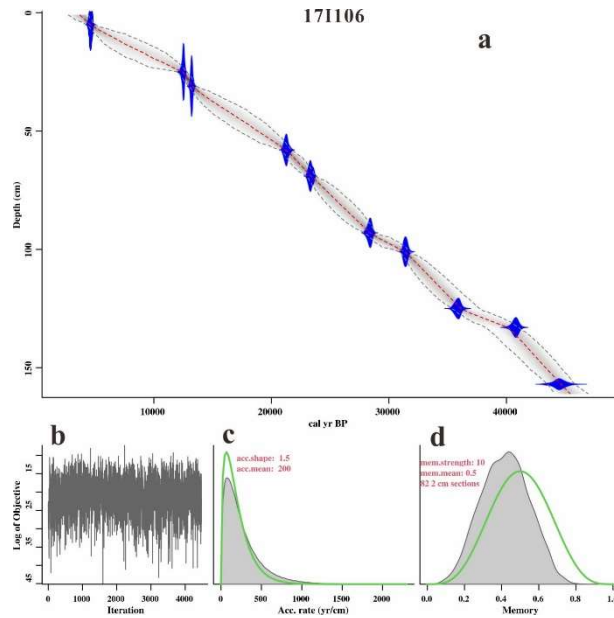
583 Zorzi, C., Sanchez Goñi, M.F., Anupama, K., Prasad, S., Hanquiez, V., Johnson, J., and Giosan, L.: Indian monsoon
584 variations during three contrasting climatic periods: The Holocene, Heinrich Stadial 2 and the last interglacial–glacial
585 transition, *Quat. Sci. Rev.*, 125, 50-60, <https://doi.org/10.1016/j.quascirev.2015.06.009>, 2015.

586 **Figure Captions**



587

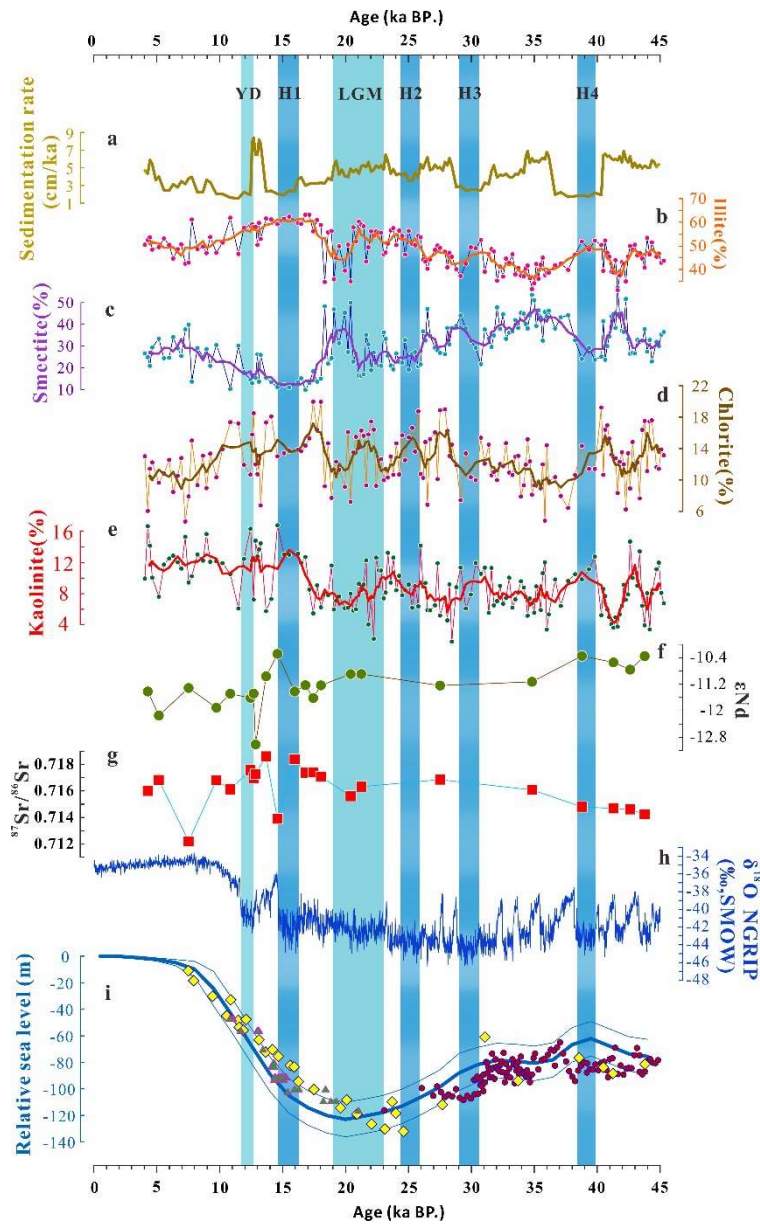
588 **Figure 1.** Geographical setting of the BoB. The locations of cores 171106 (red asterisks) and U1452 (orange diamond) are
 589 shown. On the left, the white dashed lines outline the scale of the Bengal Fan and the Nicobar Fan. The pink solid line is
 590 the “active” channel, and solid gray lines and black letters represent the turbidity channel and the reference names of the
 591 principal channels. The dotted-dashed line is the outline of the most recently active subfan (Curry et al., 2003). The solid
 592 white lines denote the two profile positions, which are shown on the right with the elevation legend.



593

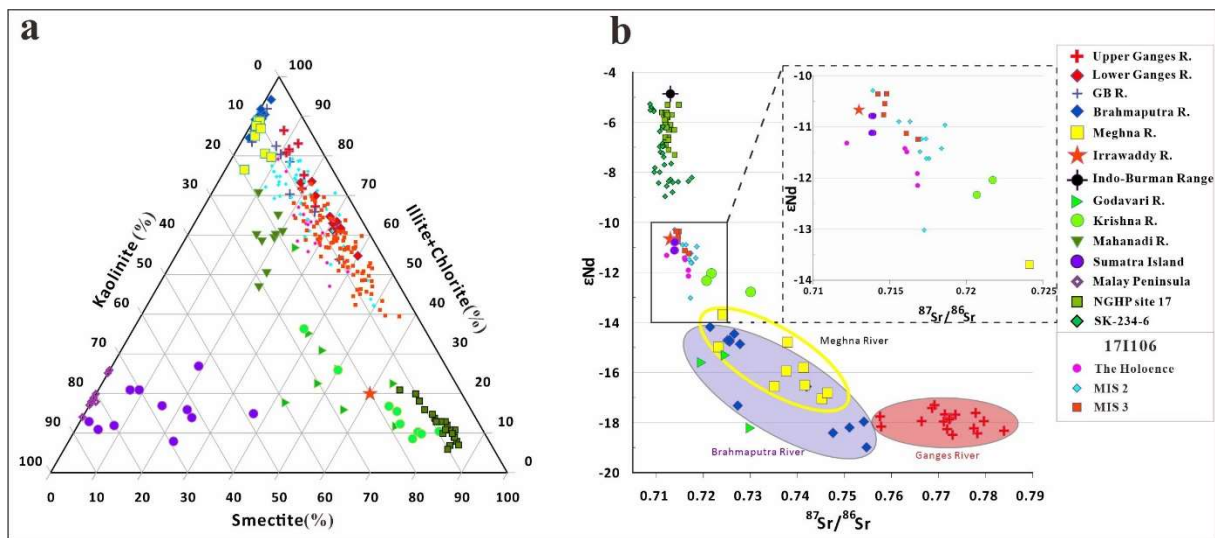
594 **Figure 2.** Age-depth model of core 171106 in the northeastern Indian Ocean. **a**, Calibrated ^{14}C dates (blue, with 2σ errors)
 595 and the resulting age-depth model (the darker gray shading indicates more likely calendar ages; the gray stippled lines

596 show 95% confidence intervals; and the red curve shows the single 'best' model based on the weighted mean age for each
 597 depth). **b**, Number of Markov chain Monte Carlo (MCMC) iterations used to generate the grayscale graphs. **c**, Prior (green)
 598 and posterior (gray) distributions of the sediment accumulation rates (the mean sediment accumulation rate was ~2
 599 years/cm). **d**, Prior (green) and posterior (gray) memory distributions (dependence of the sediment accumulation rate
 600 between neighboring depths).



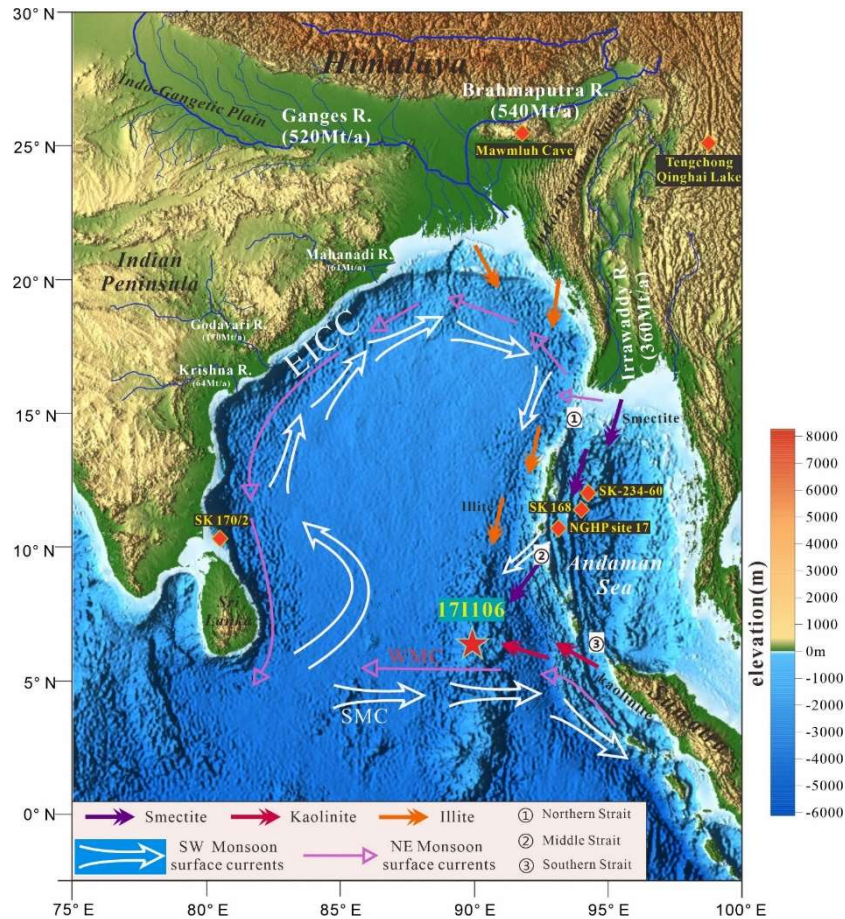
601
 602 **Figure 3.** Comparison of clay mineral and Sr-Nd isotopes data in the northeastern Indian Ocean with paleoclimate records.
 603 **a**, Sedimentation rate in core 17I106; **b, c, d, e**, illite, smectite, chlorite and kaolinite percentages in core 17I106 (thick line

604 represents a 3-point running average); **f**, **g** $^{87}\text{Sr}/^{86}\text{Sr}$ and ϵNd values of core 171106 in the northeastern Indian Ocean; **h**,
 605 $\delta^{18}\text{O}$ data of Greenland ice core NGRIP (Svensson et al., 2008); **i**, Global sea level as proxy for ice volume, reconstructed
 606 from benthic $\delta^{18}\text{O}$ (thick cyan line, thin cyan line represents the 95% confidence interval, Thompson and Goldstein, 2006),
 607 globally distributed corals (yellow dots, Waelbroeck et al., 2002) and sea level data (Triangles and red dots) collected by
 608 Grant et al.(2014) and Hanebuth et al. (2000). Blue and cyan bars represent cold climate periods of Heinrich events (H1-
 609 H4) together with Younger Dryas (YD) and the last glacial maximum (LGM), respectively.



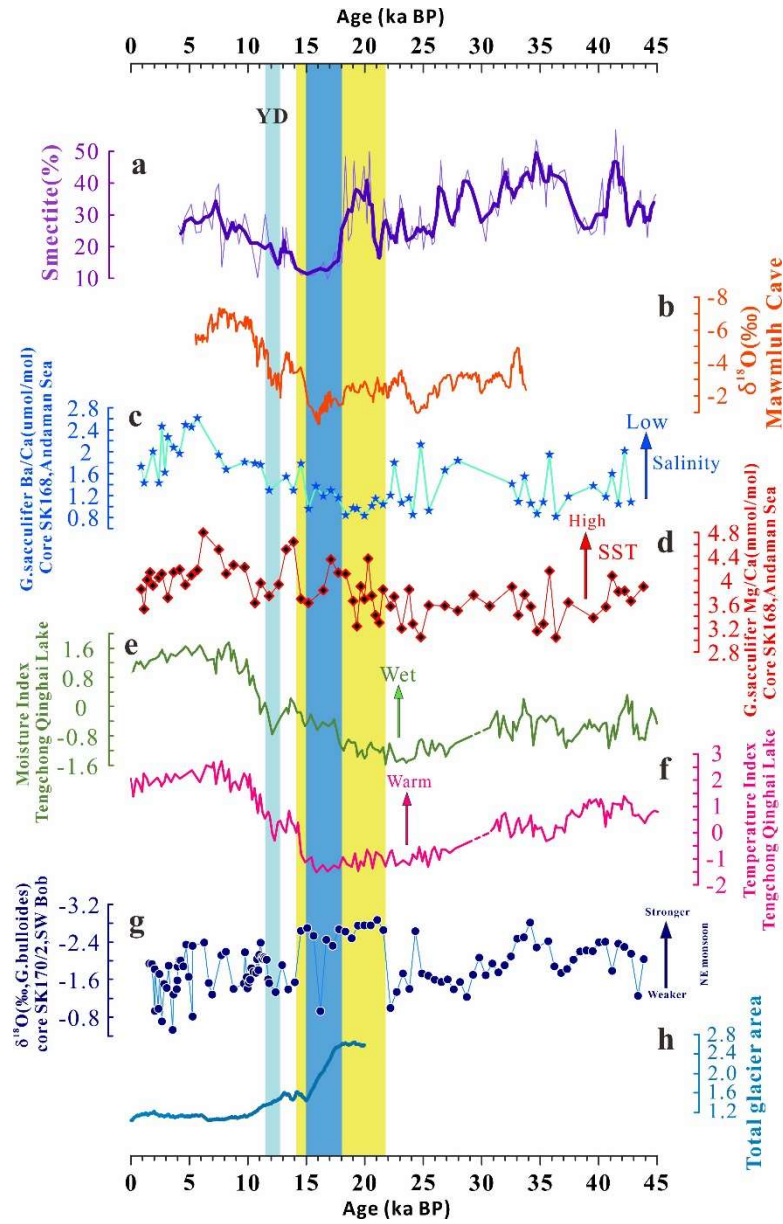
610
 611 **Figure 4.** Sediment provenance of core 171106 in the northeastern Indian Ocean. **a**, Sediment provenance discrimination
 612 diagram in the northeastern Indian Ocean. For comparison, clay mineral data obtained from sediments collected in the
 613 modern Ganges River, Brahmaputra River Lower, Ganges-Brahmaputra River Lower and Meghna River (Khan et al., 2019),
 614 Mahanadi and Krishna Rivers of Indian Peninsula (Bejugam and Nayak, 2017), Irrawaddy River (Rodolfo, 1969), and
 615 Sumatra and Malay Peninsula rivers (Liu et al., 2012) are also plotted. The referenced cores comprise NGHP Site 17 (Ali
 616 et al., 2015), representing the Irrawaddy River as the main clay mineral source in the Andaman Sea. **b**, Variations in ϵNd
 617 (0) vs. $^{87}\text{Sr}/^{86}\text{Sr}$ measured in core 171106 compared with those measured in river sediments and bulk rock samples collected
 618 around the BoB. In this diagram, we display data collected from Indian river samples (from the Godavari and Krishna
 619 Rivers) (Ahmad et al., 2009) from different parts of the modern G-B River system (Lupker et al., 2013). Measurements
 620 taken from sediments obtained from the Irrawaddy River (Colin et al., 1999), formations from the Indo-Burman ranges

621 (Licht et al., 2013) and volcanic products of Sumatra Island (Turner et al., 2001) are also plotted. The referenced cores
 622 include NGHP Sites 17 and SK-234-60, both of which indicate that the Irrawaddy River is the main Sr-Nd isotope source
 623 for the Andaman Sea.



624
 625 **Figure 5.** Map showing dispersal patterns of the BoB clay minerals for core 171106. The locations of core 171106 (red
 626 asterisks) and of the reference core and sites are shown: SK 170/2 in the northern BoB, SK-168, SK-234-60, NGHP site
 627 17 in the western Andaman Sea, and Mawmluh Cave in northeastern India and Tengchong Qinghai Lake in China are
 628 represented by orange diamonds. The orange, purple and red arrows represent the main dispersal directions of illite,
 629 smectite and kaolinite when the fluvial sediments were discharged into core 171106. The white and red arrows denote the
 630 SW and NE monsoon currents, respectively. In the western BoB, the East Indian Coastal Current (EICC) reverses annually
 631 with the monsoon wind (Schott and McCreary, 2001). In the lower-latitude regions of the BoB, monsoon-driven currents
 632 flow eastward in summer to form the summer monsoon current (SMC) and westward in winter to form the winter monsoon

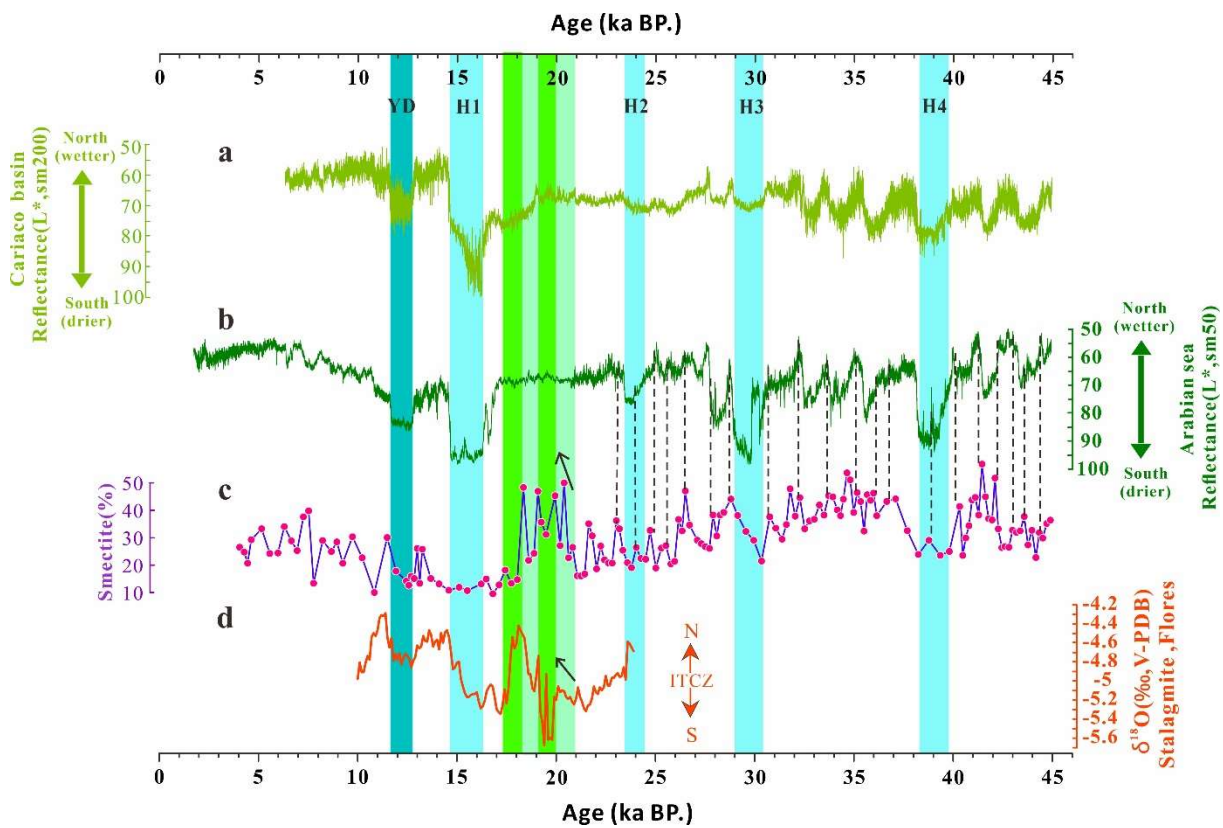
633 current (WMC) (Shankar et al., 2002). The elevation legend is shown to the right of this figure.



634

635 **Figure 6.** Comparison of smectite percentages in core 171106 with paleoclimate records. **a**, Smectite percentages in core
 636 171106 (thick line represents a 3-point running average); **b**, Mawmluh Cave $\delta^{18}\text{O}$ record for the interval 33,800 to 5500
 637 years BP (Dutt et al., 2015). **c**, **d**, Ba/Ca and Mg/Ca of the mixed layer species *G. sacculifer* in core SK 168 from the
 638 Andaman Sea, which represent the surface sea salinity and temperature, and the lower salinity and higher temperature
 639 showed a strong SW monsoon (Gebregiorgis et al., 2016). **e**, **f**, Moisture index and temperature index from pollen records
 640 from Tengchong Qinghai Lake, respectively (Peng et al., 2019; Zhang et al., 2020). **g**, $\delta^{18}\text{O}$ variability record of planktic

641 foraminifera *Orbulina universa* obtained from core SK 170/2 recovered from the southwestern Bay of Bengal, which
 642 represents the strength of the NE monsoon (Gautam et al., 2020). **h**, Ratio of the modeled total glacier area over the southern
 643 parts of the Himalayan-Tibetan orogen to the present level (Yan et al., 2020). Yellow, blue and cyan bars represent the
 644 strong NE monsoon period shown by line **g**, the main periods of glacier melting in the southern Himalayas shown by line
 645 **h** and the cold climate periods of the Younger Dryas (YD).



646
 647 **Figure 7.** Comparison of smectite percentages with ITCZ north-south shift records. **a**, L* represents the ITCZ shift from
 648 the Cariaco Basin (Deplazes et al., 2013); **b**, L* represents the ITCZ shift from the Arabian Sea (Deplazes et al., 2013); **c**,
 649 Smectite percentages in core 17I106; **d**, Stalagmite $\delta^{18}\text{O}$ record from Flores (Ayliffe et al., 2013). The gold dotted line
 650 denotes the connection between the northward movement of the ITCZ and the peak smectite percentage, and the series of
 651 color bars from 21-18 ka represent the ITCZ-shift periods recorded in **d**. The green bars represent the consistent periods
 652 shown in **c** and **d** in the late LGM, and the black arrows in **c** and **d** indicate great differences between the smectite
 653 percentages and ITCZ record in the EIO.

654 **Table 1.** Carbon-14 and calibrated calendar ages of mixed planktonic foraminifera measured in core 17I106 in the
655 northeastern Indian Ocean.

Number	Depth (cm)	Materials	Measured ^{14}C age (yr BP, $\pm 1\sigma$)	Calendar median age (yr BP)
1	5	mixed planktonic foraminifera	4160 \pm 30	4053
2	25	mixed planktonic foraminifera	10690 \pm 40	11880
34	31	mixed planktonic foraminifera	11460 \pm 40	12801
4	58	mixed planktonic foraminifera	17910 \pm 50	20710
5	69	mixed planktonic foraminifera	20050 \pm 60	23183
6	93	mixed planktonic foraminifera	24590 \pm 90	27883
7	101	mixed planktonic foraminifera	27820 \pm 120	31074
8	125	mixed planktonic foraminifera	31820 \pm 200	35455
9	133	mixed planktonic foraminifera	36370 \pm 280	40434
10	157	mixed planktonic foraminifera	42190 \pm 560	44167

656